Article

A Mitochondria-Targeted Ratiometric Biosensor for pH Monitoring and Imaging in Living Cells with Congo-Red-Functionalized Dual-Emission Semiconducting Polymer Dots

Junyong Sun, Pinghua Ling, and Feng Gao

Anal. Chem., **Just Accepted Manuscript** • DOI: 10.1021/acs.analchem.7b03154 • Publication Date (Web): 17 Oct 2017

A Mitochondria-Targeted Ratiometric Biosensor for pH Monitoring and Imaging in Living Cells with Congo-Red-Functionalized Dual-Emission Semiconducting Polymer Dots

Junyong Sun, Pinghua Ling, and Feng Gao*

Laboratory of Functionalized Molecular Solids, Ministry of Education, Anhui Key Laboratory of Chemo/Biosensing, Laboratory of Optical Probes and Bioelectrocatalysis (LOPAB), College of Chemistry and Materials Science, Anhui Normal University, Wuhu 241000, P. R. China

*Corresponding author. Phone/Fax: +86-553-3937137. E-mail: fgao@mail.ahnu.edu.cn.

ABSTRACT

The accurate and sensitive monitoring and imaging of mitochondrial pH in living cells play vital roles in chemical biology and biomedicine. Herein, we design a novel ratiometric fluorescent chemical probe for monitoring and imaging pH of mitochondria in living cells based on congo-red (CR)-modified dual-emission semiconducting polymer dots (Pdots) via a competitive fluorescence resonance energy transfer (FRET) mechanism. The Pdots are synthesized by triphenylphosphonium (TPP)-modified polyoxyethylene nonylphenylether (CO-520), Poly(9,9-dioctylfluorenyl-2,7-diyl) (PFO), poly(9,9-dioctylfluorene)-co-(4,7-di-2-thienyl-2,1,3-benzothiadiazole) (PF-DBT5), and poly(styrene-co-maleic anhydride) (PSMA) via nanoprecipitation method, and the prepared Pdots are further chemically linked with pH-sensitive, non-fluorescent CR to obtain the mitochondria-targeted pH fluorescent probes. This Pdots-based probe consists of two luminescent components including PFO and PF-DBT5 as fluorescence donors, a acid-base indicator CR as energy acceptor, and TPP as mitochondria-targeting group. At different pH region, the FRET efficiency between CR and PFO, or CR and PF-DBT5 can be modulated. This probe exhibits good biocompatibility, wide pH detection range from 2.57 to 8.96, good reversibility, high selectivity and excellent photostability for pH monitoring. This probe allows for detecting and imaging of mitochrondrial pH in the living cells with satisfactory results.

INTRODUCTION

Mitochondria, a major subcellular organell with a cystic bilayer-membrane structure as the metabolic powerhouse of the cell, plays pivotal roles in cellular metabolism functions and is involved in different essential physiological processes such as cell energy production, apoptosis, cell signaling, and calcium homeostasis.[1] The unique functions of mitochondria strongly depend on the existed microenvironments of mitochondria, especially the mitochondrial pH (pH_{mit}).[2,3] The mitochondrial pH_{mit} can directly effect a variety of biochemical processes and reflects the functional viability of the organelle.[2,3] The pH_{mit} value has to be strictly controlled within a narrow range, and variation of the normal pH_{mit} may lead to mitochondrial dysfunction and therefore results in many diseases including neurodegenerative diseases, Reye's syndrome cancers, and cardiovascular diseases.[4-6] To elucidate the mitochondria-relevant biological events, it is therefore crucial to develop accurate and sensitive methods for real-time monitoring pH_{mit} dynamics in living cells in chemical biology.

Comparing to other detection techniques such as electrochemical methods and functionalized proteins,[7, 8] fluorescent chemical probes have been widely proven to be effective tools for sensing and imaging biologically relevant species, including mitochondrial pH, in vitro and in vivo because of their intrinsic superiorities including simple operation, high sensitivity and selectivity, non-destructive detection, as well as in-situ imaging.[9-15] Up to date, a variety of synthesized organic molecules, nanoparticles, and fluorescent proteins have been reported for monitoring pH_{mit} in living cells.[16-23] However, in contrast to these single fluorescence-intensity-based fluorescent sensors, ratiometric fluorescent probes have attracted increasing attentions for precise and quantitative measurement of pH because they can more efficiently reduce the output signal fluctuations induced

by poor expression, cell movement, optical focusing, concentration and optical path length, and environmental conditions through the ratiometric self-calibration of the dual-emission band.[24-29] Thus, it is still a great challenge and highly desirable to develop new fluorescent probes with high brightness, favorable biocompatibility, significant colour change for pH monitoring and real-time imaging in mitochondria of living cells.

Semiconducting polymer dots (Pdots) derived from fluorescent conjugated polymer[30-33]display unqiue characteristics which are very favorable for fluorescence sensing and imaging, including high single-particle brightness, excellent photostability and low cytotoxicity,[33-36] and have been exploited in sensing,[37-44] imaging[35,45-50] and photodynamic therapy.[51,52] However, modified Pdots via tuning the surface chemistry as subcellular targeting probe for mitochondrial pH monitoring has not been reported so far to the best our knowledge. In this work, we designed the first example of pH-responsive and mitochondria-targeted functionalized Pdots for pH_{mit} monitoring and imaging in living cells (Scheme 1).

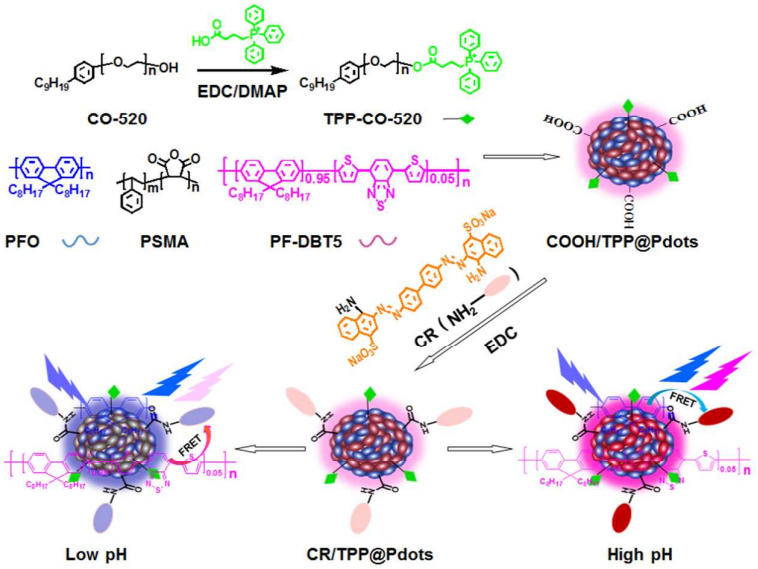

Scheme 1. Schematic illustration of the designed mitochondria-targeted Pdots for ratiometric detection of pH_{mit}.

As shown in Scheme 1, prior to preparing fluorescent Pdots, mitochondria-targeting group, triphenylphosphonium (TPP) was linked to polyoxyethylene nonylphenylether (CO-520) to obtain TTP-CO-520. And then, TTP-CO-520, Poly(9,9-dioctylfluorenyl-2,7-diyl) (PFO), poly(9,9-dioctylfluorene)-co-(4,7-di-2-thienyl-2,1,3-benzothiadiazole) (PF-DBT5), and poly(styrene-co-maleic anhydride) (PSMA) were used as raw materials to synthesize fluorescent Pdots, COOH/TPP@Pdots with nanoprecipitation method. The obtained Pdots are enriched with carboxy groups and mitochondria-targeting group. Thereafter, pH-sensitive and non-fluorescent indicator, congo red (CR), was further chemically linked to the as-prepared COOH/TPP@Pdots through typical carbodiimide (EDC)-coupling-chemistry to obtain mitochondria-targeted, pH sensitive, ratiometric fluorescent probes, CR/TPP@Pdots. The CR/TPP@Pdots exhibited attractive mitochondria-targeting ability, and high accurancy and sensitivity for monitoring pH, providing a reliable approach for ratiometric sensing and real-time imaging of mitochondrial pH in living cells.

EXPERIMENTAL SECTION

Chemicals and Instrumentals. Poly(9,9-dioctylfluorenyl-2,7-diyl)-end-capped with dimethylphenyl (PFO; average MW, 89 000; polydispersity, 2.3) was procured from ADS Dyes, Inc. (Quebec, Canada). Poly(9,9-dioctylfluorene)-co-(4,7-di-2-thienyl-2,1,3-benzothiadiazole) (PF-DBT5) is donated by Prof. Changfeng Wu from South University of Science And Technology of China. (3-Carboxypropyl) triphenylphosphonium bromide (TPP-COOH), congo red (CR), nigericin, and 4-dimethylaminopyridine (DMAP) were bought from Aladdin (Shanghai, China). Poly(styrene-co-maleic anhydride) (PSMA), polyoxyethylene nonylphenylether (CO-520, average MW 441), tetrahydrofuran (THF, anhydrous, ≥99.9%, inhibitor-free),

2-(4-(2-hydroxyethyl)-1-piperazinyl) ethanesulfonic acid buffer (HEPES) and 1-ethyl-3-[3-dimethylaminopropyl] carbodiimide hydrochloride (EDC·HCl) were all purchased from Sigma-Aldrich. Dulbecco's-modified Eagle's medium (DMEM) was procured from Hyclone (Logan, UT). All reagents and solvents were used as received from commercial suppliers without further purification. Ultrapure water with a resistivity greater than 18.25 MΩ cm was used throughout this study.

The fluorescence and UV-vis absorption spectrum was recorded on a LS-55 spectrophotometer (PerkinElmer, USA) and a Lambda-35 UV-Vis spectrophotometer (PerkinElmer, USA), respectively. Luminescence lifetime and quantum yield measurements were carried out on a FLS 920 spectrofluorometer (Edinburgh Instruments, UK). A ZS90 Zetasizer Nano instrument (Malvern, UK) was used to measure the hydrodynamic size and zeta potential. The morphology of Pdots was characterized with a HT-7700 transmission electron microscope (Hitachi, Japan) operating at an accelerating voltage of 100 kV. The images of Raw 264.7 cells were captured using a confocal laser scanning microscope (Leica, SP8, Germany).

Preparation of TTP-CO-520 and COOH/TPP@Pdots. The TPP-CO-520 was synthesised by DMAP-catalyzed reaction according to previously reported literature with modified procedures.[53] Typically, CO-520 (10 mg), TPP-COOH (16 mg), EDC·HCl (5 mg) and DMAP (1 mg) were co-dissolved in a 20 mL glass vial with 10 mL of anhydrous DMF. After magnetically stirring for 24 h, the TPP-modified CO-520, TPP-CO-520 was obtained. The polymer TPP-CO-520A with a concentration of 1 mg mL^{-1} was stored at 4 ^{o}C for further use.

The COOH/TPP@Pdots was further synthesized with slightly modified procedures reported previously. [47,54] The polymers PFO, PF-DBT5 and PSMA were dissolved in anhydrous THF to

obtain 1.0 mg mL^{-1} stock solutions under vigorous sonication, respectively. A 3 mL homogeneous THF solution containing PFO (42 μg mL^{-1}), PF-DBT5 (8 μg mL^{-1}), PSMA (16 μg mL^{-1}) and TPP-CO-520 (4 μg mL^{-1}) was quickly injected into 10 mL ultrapure water and sonicated for 5 min, and then THF was removed by reduced pressure distillation to get colloidal solution of Pdots. After that, the as-prepared colloidal solution was filtered through a 0.22 μm membrane filter to remove any formed aggregates and then concentrated with a centrifugal filtration (Amicon Ultra-4; MWCO: 100 kDa) to obtain 50 μg mL^{-1} Pdots solution. The prepared Pdots solution was stored at 4°C for further functionalization.

Preparation of CR/TPP@Pdots. The CR/TPP@Pdots were obtained by EDC-mediated coupling of COOH/TPP@Pdots with CR according to previously reported literature.[55] Typically, 100 μL of 5% PEG (w/v) and 100 μL of HEPES (1.0 M) were added into 5 mL COOH/TPP@Pdots solution (50 μg mL^{-1}) and mixed well on a vortex. Then, 150 μL of CR (10 mg mL^{-1}) was added into the above mixture to ensure that only an amino group of CR was involved into the reaction. Thereafter, 100 μL of freshly prepared EDC solution (10 mg mL^{-1}) was added and the final mixture was magnetically stirred for 4 h at room temperature. After the mixture was followed by blocking with 100 μL of 10% BSA at 37 ^{o}C for 20 min, the CR/TPP@Pdots was obtained via centrifugation with five times and stored at 4°C for further use.

Procedures for pH Detection. An equivalent amount of 10 μL of CR/TPP@Pdots (50 μg mL^{-1}) solution was put into a series of 0.6 mL colorimetric tubes and diluted to 200 μL using HEPES buffers (20 mM) with various pH values, respectively. After incubated for 10 min at 37 ^{o}C, the fluorescence measurements were performed with 380 nm light excitation, respectively.

Cell Culture and Imaging. RAW 264.7 murine macrophages were cultured in Dulbecco's modified Eagle's medium (DMEM) containing 10% FBS (WelGene), penicillin (100 units mL^{-1}), and streptomycin (100 μg mL^{-1}) at 37 ^{o}C in a humidified atmosphere containing 5% CO_2. For the subcellular location of probes, RAW 264.7 cells were incubated with CR/TPP@Pdots (2.5 μg mL^{-1}) at 37 °C for 1 h, and then Mito-Tracker green (0.5 μM) was added into the culture medium for 10 min. The cells were washed three times with PBS before viewing. For fluorescence imaging of pH_{mit} in living cells, the cells were plated in a 24-well glass bottom plate at a seeding density of 50,000 cells per well and incubated at 37 °C, and then washed with PBS to remove non-adherent cells. Prior to fluorescent staining, the adherent macrophages were starved in serum-free DMEM for 2 h. After serum starvation, the RAW 264.7 cells were incubated with CR/TPP@Pdots (2.5 μg mL^{-1}) for 1 h, followed by a standard washing program to remove the extracellular probes. Prior to image, the cells were further incubated with DMEM containing high-K^+ and 10 mM nigericin at various pH values for 15 min.

MTT Assay. The cytotoxicity of probe was tested with RAW 264.7 cells by MTT assay. Typically, the cells with a density of 10^4 cell/well were incubated for 24 h in a 96-well microtiter plate. After the cells were incubated with 100 μL culture medium containing different concentrations of CR/TPP@Pdots for 48 h, MTT (50 μL, 1 mg mL^{-1}) was added to the well and incubated at 37 °C for 4 h, and then 100 μL of dimethyl sulphoxide was added to each well. After vibrating for 15 min, the well was measured to obtain the relative cell viability (%) by $(A_{test}/A_{control})\times100\%$ at 490 nm.

RESULTS AND DISCUSSION

Design and Characterization of CR/TPP@Pdots. In order to design dual-emission ratiometric

fluorescent Pdots, we choose polymers PFO and PF-DBT5 as the luminescent components to prepare dual-emission semiconducting polymer nanoparticles due to the large wavelength difference between their emission spectra (Figure 1A, curve c, d) and almost total absorption spectra overlapping (Figure 1A, curve a, b), which provides a precondition to prepare single-excitation, dual-emission ratiometric probes. In addition, as shown in Figure 1A, little spectral overlap between the emission spectrum of PFO (curve c) and the absorption spectrum of PF-DBT5 (curve b) is observed, suggesting that the intermolecular energy transfer within single Pdot can happen and therefore endow Pdots with dual-emission characteristics using excitation wavelength of 380 nm. To achieve mitochondria-targeted purpose, the mitochondria-targeting groups, TPP molecules were anchored on polymer CO-520 to obtain amphiphilic polymer TPP-CO-520. Based on the above considerations, polymers TPP-CO-520 and PSMA were further blended with semiconducting polymers PFO and PF-DBT5 to get COOH/TPP@Pdots. To evaluate the compact structure of the obtained COOH/TPP@Pdots, a leaching test was performed by comparing the absorption spectra of COOH/TPP@Pdots with the absorption spectra of the centrifugal filtrate COOH/TPP@Pdots solution after ultrafiltration. The centrifugal filtration of COOH/TPP@Pdots was obtained by centrifuging at 3500 rpm for 5 min through a centrifugal filtration device (Amicon Ultra-4 Centrifugal Filter with a molecular weight cutoff of 100 000). Figure S1 (Supporting Information) shows the absorption spectra of COOH/TPP@Pdots and corresponding filtrate obtained by ultrafiltration, respectively. As shown in Figure S1, the absorption spectra of centrifugal filtration of COOH/TPP@Pdots displays almost a straight line and no obvious absorption peaks are observed, suggesting that the leaching of polymers embedded in the composite Pdots is negligible due to the hydrophobic characteristics of the conjugated polymers

and covalent conjugation of TPP-CO-520. The COOH/TPP@Pdots were further covalently linked with pH-sensitive indicator, CR to obtain the final functionalized Pdots, CR/TPP@Pdots to realize pH sensor. As expected, the as-prepared fluorescent COOH/TPP@Pdots show two emission bands when excited with 380 nm, locating at the shorter wavelengths region originated from PFO emission at 442 and 468 nm (blue region), and the longer wavelength originated from PF-DBT5 emission at 616 nm (red region) (Figure 1B). The absorption cross section of the single particle is estimated to be ca. 5.73×10^{-13} cm^2, and the fluorescence quantum efficiency is estimated to be 0.487. The mitochondria-targeting groups, TPP molecules on the surface of Pdots can be confirmed by NMR, SEM-EDS analysis, and UV absorption spectrum. As shown in Figure 1C, the COOH/TPP@Pdots exhibit characteristic proton NMR signal of TPP at 7.748 ppm, which is close to the reported value.[56] In addition, EDS elemental analysis clearly shows that the TPP molecules were loaded on the Pdots surface (Figure S2, supporting information). From the UV−vis spectra shown in Figure 1D, TPP-CO-520(curve b) and COOH/TPP@Pdots (curve c) display a characteristic absorption band of TPP (curve a) appeared at 267 nm. The average number of TPP molecules anchored on Pdots was calculated to be ca. 325 per Pdots. These results indicate the TPP was successfully modified on the probe surface.

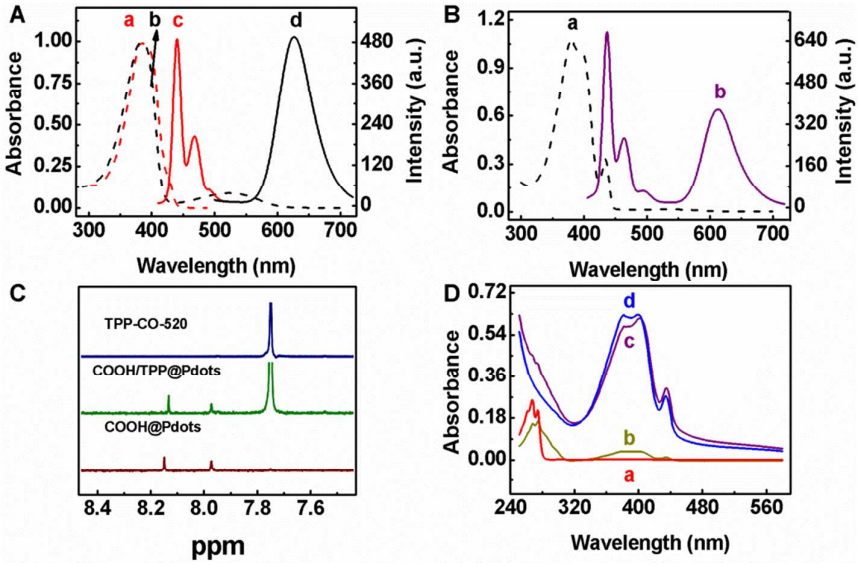

Figure 1. (A) Absorption (a, b) of PFO and PF-DBT5 in THF solution and emission spectra (c, d) of PFO and PF-DBT5 Pdots in aqueous solution. (B) Absorption (a) and emission (b) spectra of COOH/TPP@Pdots. (C) Proton NMR spectra of TPP-CO-520, COOH/TPP@Pdots and COOH@Pdots. (D) UV-visible absorption spectra of TPP (a), TPP-CO-520 (b), COOH/TPP@Pdots (c), and COOH@Pdots (d).

In order to further verify the formation of the target functional Pdots, transmission electron micrographs (TEM), dynamic light scattering (DLS) and agarose gel were employed to investigate the fabrication process of CR/TPP@Pdots. As shown in Figure 2, the TEM images show that both COOH/TPP@Pdots (Figure 2A) and CR/TPP@Pdots (Figure 2B) exhibit highly spherical monodisperse with dimensions of approximately 21 nm and 26 nm, respectively. This result is accordance with the results of DLS measurements (Figure S3), indicating the successful synthesis of CR/TPP@Pdots. Figure 2C display the agarose gel electrophoresis lanes of different COOH/TPP@Pdots or mixtures. As shown in this figure, COOH/TPP@Pdots and the mixtures including COOH/TPP@Pdots and EDC, and COOH/TPP@Pdots and CR have the same positions on the gel. However, when mixing COOH/TPP@Pdots, CR and EDC, in which CR can link with

COOH/TPP@Pdots via EDC reaction, the lane shows lower migration rate, indicating the CR molecules are anchored on Pdots surface.

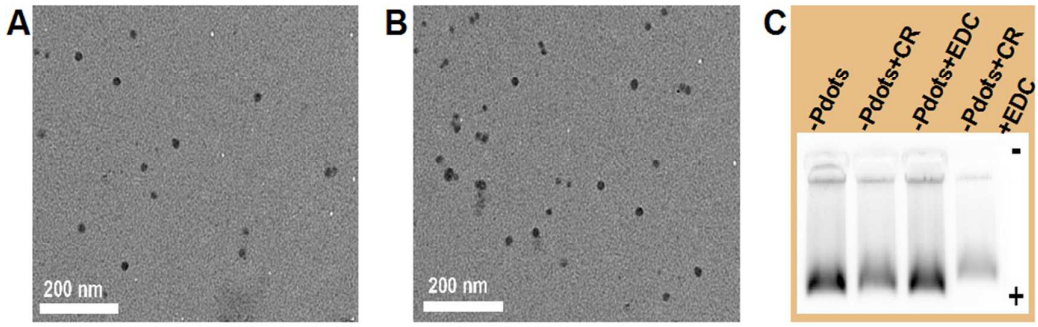

Figure 2. TEM images of COOH/TPP@Pdots (A) and CR/TPP@Pdots (B), and Agarose gel electrophoresis assays of different COOH/TPP@Pdots composites (C).

Ratiometric pH Sensing Mechanism of CR/TPP@Pdots. As we know, congo red, the sodium salt of benzidinediazo-bis-1-naphthylamine-4-sulfonic acid, is a non-fluorescent acid-base indicator with a pKa value of 5.5,[57] and its chemical structural changes are closely associated with the pH of solution due to the protonation/deprotonation processes.[58] Fluorescence spectra were firstly performed to investigate the fluorescent properties of CR/TPP@Pdots in HEPES buffer solution with different pH values. As shown in Figure 3A, when the pH values change from 8.96 to 2.57, no obvious changes in the intensities of blue emission region originated from PFO component in Pdots, while dramatical changes in the intensities of red emission band originated from PF-DBT5 component in Pdots were observed when excited with 380 nm. This suggests that a ratiometric sensor of can be constructed using the blue fluorescence in blue region as reference signal while the red fluorescence as report signal. These experimental results can be explained by the efficiency of intermolecular fluorescence resonance energy transfer within particles as follows. As shown in Figure 3B, with the pH values changing from base region to acid region, the absorption peak

location of CR displays red-shift accompanying with gradually decreasing absorbance, which will affect the extent of spectra overlap between the donor and the acceptor and therefore influence the efficiency of the FRET process. Figure 3C displays the spectra overlap between absorption spectra of CR and fluorescence spectra of Pdots at pH 8.96 and 2.57, respectively. As depicted in Figure 3C, with the decreasing pH value decreasing from 8.96 to 2.57, the spectral overlap between the emission of PFO of Pdots and the absorption of CR was gradually decreased, while the spectral overlap between the emission of PF-DBT5 of Pdots and the absorption of CR exhibited an obvious enhancement. In order to compare the FRET efficiency of PF-DBT5 and CR at different pH, the FRET efficiencies at two typical pH values were calculated. At pH 8.96 (basic region), the FRET efficiency was calculated to be 5.2%, which is much lower than the value of 73.4% at pH 2.57(acidic region). This result is good agreement with the situation of spectral overlay at the two pH values. To further confirm the FRET mechanism between the luminescent components of Pdots and CR, time-resolved fluorescence measurements were performed by collecting the emission intensities at 616 nm. As shown in Figure 3D, the fluorescence lifetime is estimated to be 3.40 ns for CR/TPP@Pdots and 4.67 ns for COOH/TPP@Pdots, respectively. This suggests that CR can interact with the excitation state of COOH/TPP@Pdots, supporting the presence of FRET from Pdots to CR, which is consistent with the predictions of the energy transfer model demonstrated above.

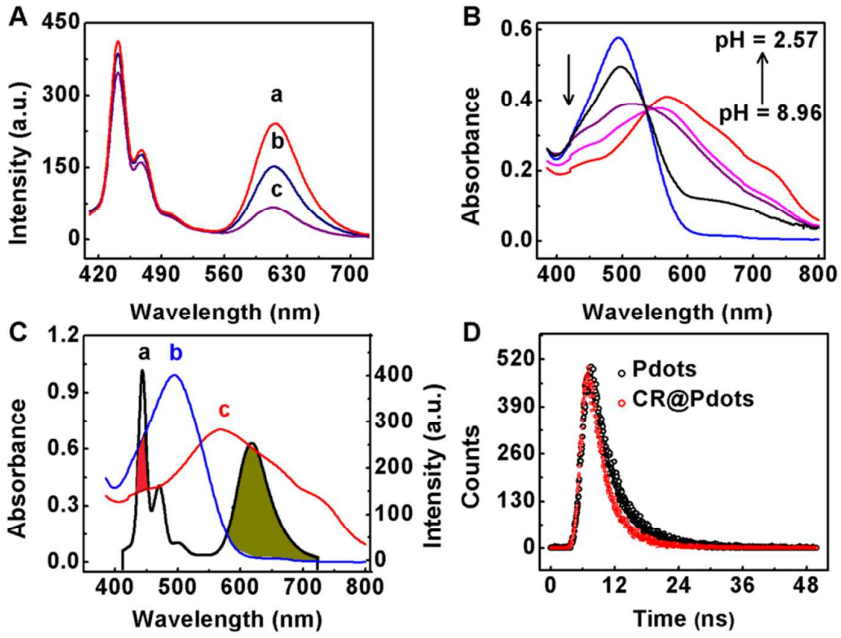

Figure 3. Fluorescence emission spectra of CR/TPP@Pdots (2.5 μg mL^{-1}) at pH 8.96 (a), 6.01 (b) and 2.57 (c) with an excitation of 380 nm. (B) UV–Vis absorption spectra of CR at pH 8.96 (a), 6.77 (b), 5.75 (c), 4.03 (d) and 2.57 (e). (C) The spectra overlap between emission spectra of Pdots (a) and absorption spectra of CR with pH 8.96 (b) or and 2.57 (c). (D) Time-resolved fluorescence spectra of COOH/TPP@Pdots (black dot line) and CR/TPP@Pdots (red dot line).

Ratiometric Fluorescence Detection of pH in Buffer Solution. The feasibility of the designed fluorescent ratiometric probe for pH detection was examined in HEPES buffer solution with various pH values. As shown in Figure 4A, upon increasing pH value from 2.57 to 8.96, the intensities of red emission band of CR/TPP@Pdots at 616 nm was significantly increased, while those of blue emission bands at both 442 and 468 nm are nearly silent. In the meantime, a noticeable color changing from blue to magenta with the changing of pH value was observed under UV lamp, indicating the pH can also be identified by the naked eyes (inset in Figure 4A). The relative fluorescence intensity ratios (I_{616}/I_{442}) showed a good linear proportion to the pH values in the range

from 2.57 to 8.96 with a correlation coefficient of 0.9978 (Figure 4B). Figure 4C shows the reversibility of CR/TPP@Pdots for cyclic detection of pH at 2.5 and 9.0, the CR/TPP@Pdots shows excellent reversibility between pH 2.5 and pH 9.0, which is attributed to the inherent characteristic of fast protonation/deprotonation process of CR[57,58] and excellent stability of the fluorescent probe. Furthermore, the photostability of the CR/TPP@Pdots at different pH values were investigated. Figure 4D demonstrates the individual time-dependent absolute fluorescence intensity of blue (a, c, e) and red (b, d, f) emission of CR/TPP@Pdots in different pH under the irradiation of a 365 nm UV lamp. We can see from this figure that both the individual fluorescence intensity and the ratio (inset of Figure 4D) of CR/TPP@Pdots in different pH buffers did not show significant changes with a duration of 130 min, indicating that CR/TPP@Pdots exhibited excellent photostability. This result was in substantial agreement with the reports in the previous literature. [21,24] In all, the prepared CR/TPP@Pdots exhibit good stability and can be used for long-term monitoring of pH.

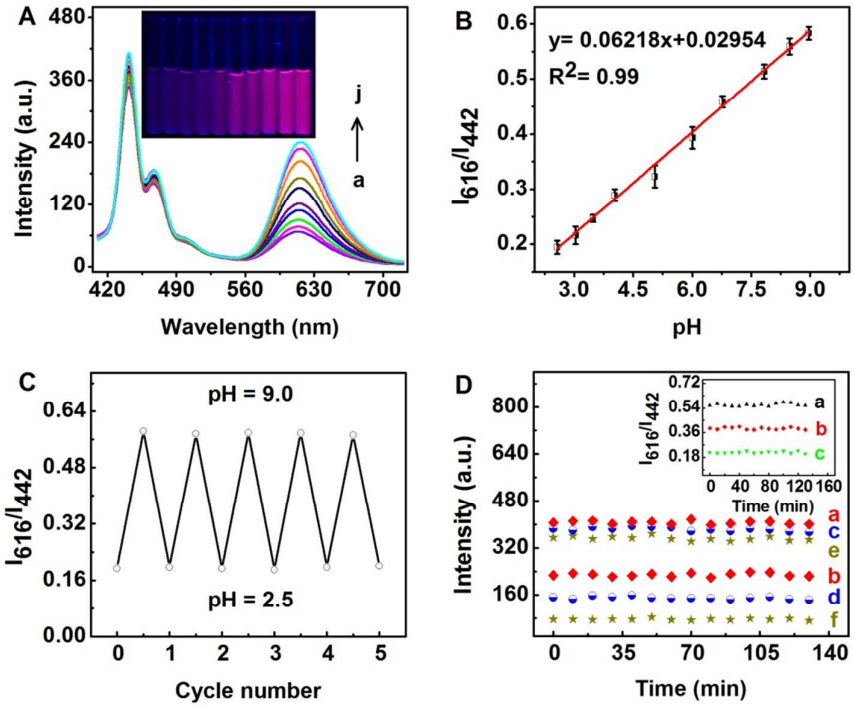

Figure 4. (A) Fluorescence emission spectra of CR/TPP@Pdots with an excitation of 380 nm in

20.0 mM HEPES buffer solution at pH 2.57 (a), 3.04 (b), 3.48 (c), 4.03 (d), 5.05 (e), 6.01 (f), 6.77 (g), 7.83 (h), 8.48 (i) and 8.96 (j). The inset photos are the corresponding colors under a 365 nm UV lamp. (B) Plot of the relative fluorescence intensity ratios (I_{616}/I_{442}) in response to pH values. (C) The intensity ratios (I_{616}/I_{442}) of CR/TPP@Pdots upon repeatedly switching pH from 2.5 to 9.0. (D) The time-dependent absolute FL intensity of blue (a, c, e) and red (b, d, f) emission of CR/TPP@Pdots with a 365 nm UV lamp in 20.0 mM HEPES buffer solution at pH 8.5, 6.0 and 3.0. The inset photo represents the corresponding time-dependent intensity ratios (I_{616}/I_{442}) of CR/TPP@Pdots with a 365 nm UV lamp at pH = 8.5 (a), 6.0 (b), and 3.0(c). The concentration of CR/TPP@Pdots for all experiments is 2.5 μg mL^{-1}.

In order to investigate the anti-interfering ability of CR/TPP@Pdots for pH sensing, the variations in fluorescence intensity ratios (I_{616}/I_{442}) in the presence of potential interfering substances including ions, amino acids and bioactive small molecules were examined under the same conditions. As depicted in Figure S4, comparing with the blank I_{616}/I_{442} ratio in the absence of interfering substances, no detectable variations in the I_{616}/I_{442} ratios were observed when adding different interfering species such as 100 μM of K^+, Na^+, Fe^{2+}, Ca^{2+}, Zn^{2+}, Cu^{2+}, Mg^{2+}, Hg^{2+}, Cd^{2+}, Ni^{2+}, Co^{2+}, and 5 μM of L-arginine (Arg), glutamic acid (Glu), L-cysteine (Cys), glutathione (GSH), serine (Ser), methionine (Met), valine (Val), L-tyrosine (Tyr), phenylalanine (Phe), glucose and dopamine (DA). The anti-interfering experiment reveals that CR/TPP@Pdots display the capacity for pH determination with high selectivity and can be used to monitor the pH in complex biological samples including living cells. In addition, the effects of ionic strength on the pH sensing of CR/TPP@Pdots also were investigated by adding different concentrations of NaCl to the buffer. As shown in Figure S5, the relative fluorescence intensity ratios of the present pH sensor has no

obvious change with the increasing in ionic strength, revealing the effect of ionic strength is negligible.

Cytotoxicity Measurements. To evaluate the biocompatibility and feasibility of bio-applications of CR/TPP@Pdots, an MTT assay was performed. As shown in Figure S6, the cell viability of Raw 264.7 cells was above 68.7% when the concentration of CR/TPP@Pdots was as high as up to 16 μg mL^{-1}, which is comparable with those reported previously.[59,60] This indicates that the present CR/TPP@Pdots exhibit low cytotoxicity and good biocompatibility in living systems.

Mitochondria Targeting of CR/TPP@Pdots. We first checked the mitochondrial targeting performance of the CR/TPP@Pdots nanoprobes using confocal laser scanning microscopic image. The co-localization test was carried out by co-incubating the Raw 264.7 cells with CR/TPP@Pdots and a commercially available mitochondria tracker (Mitotracker green). As seen in Figure 5, a bright fluorescence of CR/TPP@Pdots (red channel, Figure 5B) was observed, which is well-overlapped with that of Mitotracker green (green channel, Figure 5A) with a Pearson's coefficient of 0.896, suggesting that the present CR/TPP@Pdots have the mitochondria-positioning capability.

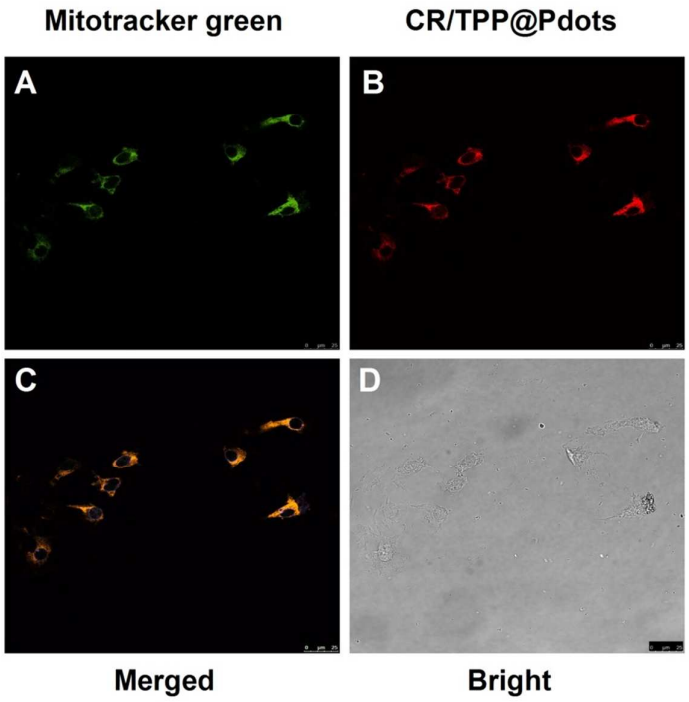

Figure 5. Confocal laser scanning microscopic images for Raw 264.7 cells incubated with DMEM (pH=7.4) containing Mito-Tracker green (0.5 μM) and CR/TPP@Pdots (2.5 μg mL^{-1}). (A) Green fluorescence of Mito-Tracker green using excitation wavelengths of 490 nm. (B) Red fluorescence of CR/TPP@Pdots using excitation wavelengths of 380 nm. (C) Merge image of (A) and (B). (D) Bright field images. Imaging windows of green channel and red channel with 510-570 nm and 590–640 nm. Scale bar represents 25 μm.

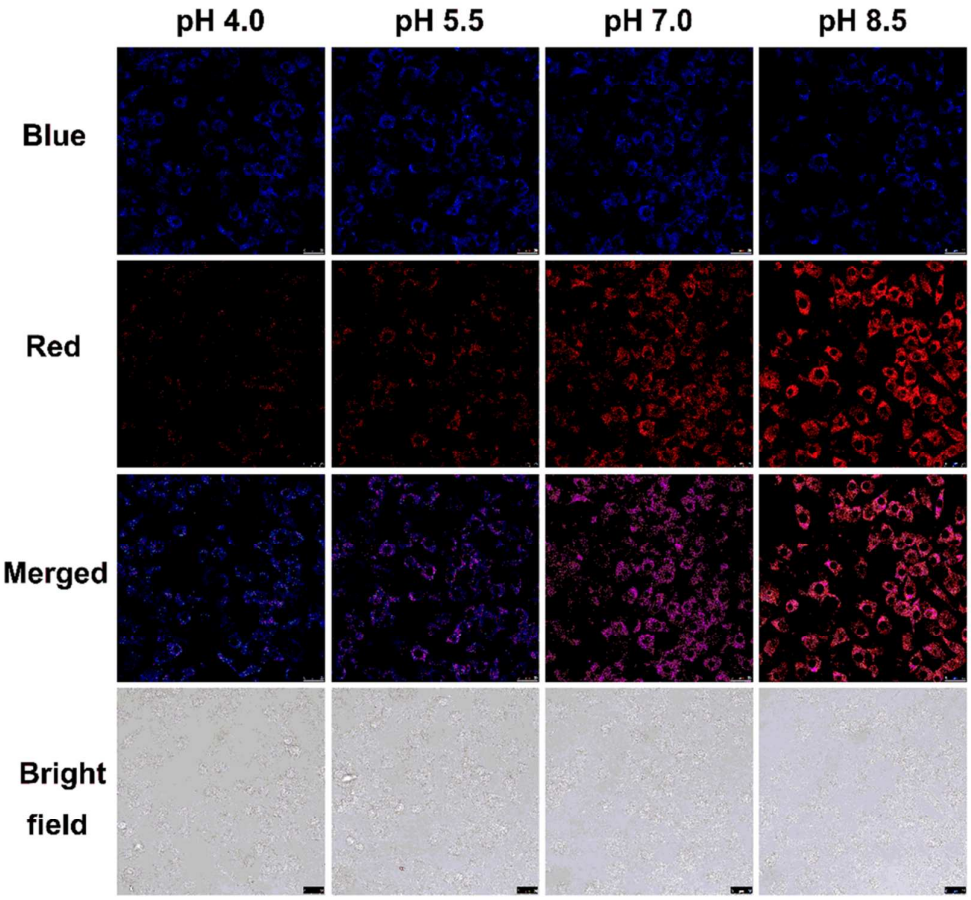

Figure 6. Confocal microscopy images of Raw 264.7 cells were incubated CR/TPP@Pdots (2.5 μg mL^{-1}) at pH 4.0, 5.5, 7.0 and 8.5. The images of blue channel and red channel with the emission windows of 420−470 nm and 590−640 nm; Scale bar represents 25 μm.

Fluorescence Imaging of pH_{mit} in Living Cells. To investigate the potential of the CR/TPP@Pdots to monitor pH in mitochondria, CR/TPP@Pdots were incubated with Raw 264.7 cells for 1 h, and the cells were then washed with pH 7.0 phosphate buffer. Thereafter, the cells were incubated in new cell culture medium containing high-K^+ and 10 mM nigericin at various pH. Nigericin, a polycyclic ether carboxylic acid compound, can readjust a rapid equilibration of the intracellular and extracellular pH as H^+/K^+ ionophore.[61,62] After incubating at 37 °C for 15 min, the cells were investigated by the confocal microscopy images. As depicted in Figure 6, the fluorescence intensities of red channel were notably enhanced with the increasing of pH from 4.0 to 8.5, while no obvious changing in fluorescence intensities were observed in the blue channel. And also, obvious color changing from blue to pink in merged channel was observed. These observations are in good agreement with spectral results in buffer solution described in above text, indicating that CR/TPP@Pdots nanoprobes could be activated by pH in the living cells. In order to quantitative detection of pH in living cells, the fluorescence intensity ratios, I_{red}/I_{blue}, of CR/TPP@Pdots were calculated by pixel-by-pixel calculation of images recorded in the red and blue channels of the Raw 264.7 cells imaging. As shown in Figure S7, the fluorescence intensity ratios showed a characteristic pH-dependent signal with a good linear relationship (R^2 =0.986) in the pH ranging from 4.0 to 8.5, indicating that CR/TPP@Pdots show the ability of to detect exogenous pH in living cells. The bright field imaging reflects the state of cells survival, and further confirms that the prepared CR/TPP@Pdots display good biocompatibility. Taking the linear detect pH range into account, the CR/TPP@Pdots have excellent performance for pH_{mit} detection not only in normal mitochondria, but also in damaged mitochondria or in pathogenic state of living cells.

CONCLUSIONS

In summary, we have provided the first example of pH-responsive and mitochondria-targeted functionalized Pdots for pH monitoring and imaging in the living cells. The CR/TPP@Pdots with

dual-emission exhibit fast response, wide pH detect range, good reversibility, high selectivity and excellent photostability as ratiometric fluorescent probes. These distinguished properties of CR/TPP@Pdots make them suitable for monitoring and imaging the pH in living systems. The nanoprobes have been successfully employed to detect and image pH_{mit} with dual-channel in the Raw 264.7 cells, and showed a good linear relationship between the fluorescence intensity ratios and pH values. We believe that rational design and functionalization of Pdots will offer an excellent strategy and platform for the detection of a wide range of various analysts in living systems.

ASSOCIATED CONTENT

Supporting Information Available:

Characterization of COOH/TPP@Pdots including EDS elemental analysis, and dynamic light scattering, leaching test of the Pdots, selectivity of CR/TPP@Pdots for pH detection, evaluation of cytotoxicity of CR/TPP@Pdots and calibration curve of intracellular pH are provided as Supporting Information. These materials are available free of charge via the Internet at http://pubs.acs.org.

AUTHOR INFORMATION

Corresponding Author

* Phone/Fax: +86-553-3937137. E-mail: fgao@mail.ahnu.edu.cn.

Notes

The authors declare no competing financial interest.

ACKNOWLEDGEMENTS

This work was financially supported by the Natural Science Foundation of China (no. 21575004, 21605001), Program for New Century Excellent Talents in University (NCET-12-0599), the project

sponsored by SRF for ROCS, SEM, and the Foundation for Innovation Team of Bioanalytical Chemistry of Anhui Province are acknowledged for supporting this work.

REFERENCES

(1) Ernster, L.; Schatz, G. *J. Cell Biol.* **1981**, *91*, 227-255.

(2) Akhmedov, D.; Braun, M.; Mataki, C.; Park, K.; Pozzan, T.; Schoonjans, K.; Rorsman, P.; Wollheim, C.; Wiederkehr, A. *FASEB J.* **2010**,*11*, 4613-4626.

(3)De Meis, L.; Tume, R. K. *Biochemistry* **1977**, *16*, 4455-4463.

(4) Ding, W. X.; Yin, X. M. *Biol. Chem.* **2012**, *393*, 547-564.

(5) Partin, J. C.; Schubert, W. K.; Partin, J. S. N. *Engl. J. Med.* **1971**, *285*, 1339-1343.

(6) Kubli, D. A.; Gustafsson, A. B. *Circ. Res.* **2012**, *111*, 1208-1221.

(7) Hesse, S.J.A.; Ruijter, G.J.G.; Dijkema, C.; Visser, J. *Biotechnology* **2000**, *77*, 5-15.

(8)Takmakov, P.; Zachek, M. K.; Keithley, R. B.; Bucher, E. S.; McCarty, G. S.; Wightman, R. M. *Anal. Chem.* **2010**, *82*, 9892-9900.

(9)Y. Yang, Q. Zhao, W. Feng, F.Y. Li, *Chem. Rev.* **2013**,*113*,192-270.

(10)Ding, C.; Zhu, A.; Tian, Y. *Acc. Chem. Res.* **2014**, *47*, 20-30.

(11)Yin, J.; Hu, Y.; Yoon, J. *Chem. Soc. Rev.* **2015**, *44*, 4619-4644

(12) Li, X.; Gao, X.; Shi, W.; Ma, H. *Chem. Rev.* **2014**, *114*, 590-659.

(13) Guo, Z.; Park, S.; Yoon, J.; Shin, I. *Chem. Soc. Rev.* **2014**, *43*,16-29.

(14)Deng, J.;Wang, K.; Wang, M.; Yu, P.; Mao, L. *J. Am. Chem. Soc.* **2017**, *139*, 5877-5882.

(15)Ueno, T.; Nagano, T. *Nat. Methods* **2011**, *8*, 642-645.

(16) Lee, M. H.; Park, N.; Yi, C.; Han, J. H.; Hong, J. H.; Kim, K. P.; Kang, D. H.; Sessler, J. L.; Kang, C.; Kim, J. S. *J. Am. Chem. Soc*. **2014**, *136*, 14136-14142.

(17)Makiko Ogata;Takeo Awaji ;Naoko Iwasaki; Risa Fujimaki; Miho Takizawa ; Kei Maruyama ;Yasuhiko Iwamoto;Yasuko Uchigata. *Biochem. Biophys. Res. Commun*. **2012**, *421*, 20-26.

(18) Llopis, J.; Mccaffery, J. M.; Miyawaki, A.; Farquhar, M. G.; Tsien, R. Y. *Proc. Natl. Acad. Sci. USA* **1998**, *95*, 6803-6808.

(19) Abad, M. F.; Di Benedetto, G.; Magalhaes, P. J.; Filippin, L.; Pozzan, T. *J. Biol. Chem*. **2004**, *279*, 11521-11529.

(20) Cao, L. X.; Zhao, Z. S.; Zhang, T.; Guo, X. D.; Wang, S. Q.; Li, S. Y.; Li, Y.; Yang, G. Q. *Chem*. *Commun*. **2015**, *51*, 17324-17327.

(21) Yang, L. M.; Li, N.; Pan, W.; Yu, Z. Z.; Tang, B. *Anal*. *Chem*. **2015**, *87*, 3678-3684.

(22) He, C. B.; Lu, K.; Lin, W. B. *J. Am. Chem. Soc*. **2014**, *136*, 12253-12256.

(23) Li, P.; Xiao,H.; Cheng, Y.; Zhang, W.; Huang, F.; Zhang, W.; Wang, H.; Tang, B. *Chem. Commun.* **2014**, *50*, 7184-7187.

(24)Shi, W.; Li, X.; Ma, H. *Angew. Chem. Int. Ed.* **2012**, *51*, 6432-6435.

(25) He, L.W.; Lin, W. Y.; Xu, Q. Y.; Wei, H. P. *ACS Appl. Mater. Interfaces* **2014**, *6*, 22326-22333.

(26) Wu, M. Y.; Li, K.; Liu, Y. H.; Yu, K. K.; Xie, Y. M.; Zhou, X. D.; Yu, X. Q. *Biomaterials* **2015**, *53*, 669-678.

(27) Ma, T.; Ma, Y.; Liu, S.; Zhang, L.; Yang, T.; Yang, H. R.; Lv, W.; Yu, Q.; Xu, W.; Zhao, Q.; Huang, W. *J. Mater. Chem. C* **2015**, *3*, 6616-6620.

(28) Chen, Y. C.; Zhu, C. C.; Cen, J. J.; Bai, Y.; He, W. J.; Guo, Z. J. *Chem. Sci*. **2015**, *6*, 3187-3194.

(29) Liu, X.; Su, Y.; Tian, H.; Yang, L.; Zhang, H.; Song, X.; W. Foley, J. W. *Anal. Chem.* **2017**, *89*, 7038-7045

(30) Wu, C.; Chiu, D. T. *Angew. Chem. Int. Ed*. **2013**, *52*, 3086-3109.

(31) Chan, Y. H.; Wu, P. J. *Part. Part. Syst. Charact.* **2014**, 3*2*, 11-28.

(32) Peng, H. S.; Chiu, D. T. *Chem*. *Soc*. *Rev*. **2014**, *44*, 4699-4722.

(33)Yu, J. B.; Rong, Y.; Kuo, C. T.; Zhou, X. H.; Chiu, D. T. *Anal*. *Chem*. **2016**, *89*, 42-56.

(34)Wu, C. F.; Bull, B.; Szymanski, C.; Christensen, K.; McNeill, J. *ACS Nano* **2008**, *2*, 2415-2423.

(35)Liu, Z. H.; Sun, Z. Z.; Di, W. H.; Qin, W. P.; Yuan, Z.; Wu, C. F. *Opt*. *Lett*. **2015**, *40*, 1242-1245.

(36)Chen, H. B.; Chang, K. W.; Men, X. J; Sun, K.; Fang, X. F.; Ma, C.; Zhao, Y. X.; Yin, S. Y.; Qin, W. P.; Wu, C. F. *ACS Appl. Mater. Interfaces* **2015**, *7*, 14477-14484.

(37)Kuo, S. Y.; Li, H. H.; Wu, P. J.; Chen, C. P.; Huang, Y. C.; Chan, Y. H. *Anal. Chem.* **2015**, 8*7*, 4765-4771.

(38) Sun, J. Y.; Wang, S. F.; Gao, F. *Langmuir* **2016**, *32*, 12725-12731.

(39) Wu, P. J.; Kuo, S. Y.; Huang, Y. C.; Chen, C. P.; Chan, Y. H. *Anal*. *Chem*. **2014**, 8*6*, 4831-4839.

(40) Sun, J.; Mei, H.; Gao, F. *Biosens*. *Bioelectron*. **2017**, *91*, 70-75.

(41) Chan, Y. H.; Jin, Y.; Wu, C.; Chiu, D. T. *Chem. Commun.* **2011**, *47*, 2820-2822.

(42) Li, Q.; Sun, K.; Chang, K.; Yu, J.; Chiu, D. T.; Wu, C.; Qin, W. *Anal. Chem.* **2013**, *85*, 9087-9091.

(43) Ye, F.; Wu, C.; Jin, Y.; Chan, Y. H.; Zhang, X.; Chiu, D. T. *J. Am. Chem. Soc.* **2011**, *133*, 8146-8149.

(44) Chan, Y. H.; Wu, C.; Ye, F.; Jin, Y.; Smith, P. B.; Chiu, D. T. *Anal. Chem.* **2011**, *83*, 1448-1455.

(45) Wu, X.; Wu, L.; Wu, I. C.; Chiu, D. T. *RSC Adv.* **2016**, *6*, 103618-103621.

(46) Wu, L.; Wu, I. C.; DuFort, C. C.; Carlson, M. A.; Wu, X.; Chen, L.; Kuo, C.-T.; Qin, Y.; Yu, J.; Hingorani, S. R.; Chiu, D. T. *J. Am. Chem. Soc.* **2017**, *139*, 6911-6918.

(47) Liu, H. Y.; Wu, P. J.; Kuo, S. Y.; Chen, C. P.; Chang, E. H.; Wu, C. Y.; Chan, Y. H. *J. Am. Chem. Soc*. **2015**, *137*, 10420-10429.

(48) Sun, J.; Mei, H.; Wang, S.; Gao, F. *Anal. Chem*. **2016**, *88*, 7372-7377.

(49) Pu, K. Y.; Shuhendler, A. J.; Rao, J. H. *Angew. Chem. Int. Ed*. **2013**, *52*, 10325-10329.

(50) Pu, K.; Mei, J. G.; Jokerst, J. V.; Hong, G. S.; Antaris, A. L.; Chattopadhyay, N.; Shuhendler, A. J.; Kurosawa, T.; Zhou, Y.; Gambhir, S. S.; Bao, Z. N.; Rao, J. H. *Adv. Mater*. **2015**, *27*, 5184-5190.

(51) Chang, K. W.; Tang, Y.; Fang, X. F.; Yin, S. Y.; Xu, H.; Wu, C. F. *Biomacromolecules* **2016**, *17*, 2128-2136.

(52) Shen, X. Q.; Li, S.; Li, L.; Yao, S. Q.; Xu, Q. H. *Chem. Eur. J*. **2015**, *21*, 2214-2221.

(53) Wu, P. J.; Chen, J. L.; Chen, C. P.; Chan, Y. H. *Chem. Commun*. **2013**, *49*, 898-900.

(54) Chen, C. P.; Wu, P. J.; Liou, S. Y.; Chan, Y. H. *RSC Adv*. **2013**, *3*, 17507-17514.

(55) Wu, C. F.; Schneider, T.; Zeigler, M.; Yu, J. B.; Schiro, P. G.; Burnham, D. R.; McNeill, J. D.; Chiu, D. T. *J. Am. Chem. Soc*. **2010**, *132*, 15410-15417.

(56) Chakraborty, A.; Jana, N. R. *J. Phys. Chem. C* **2015**, *119*, 2888-2895.

(57) Cotoruelo, L. M.; Marqués, M. D.; Díaz, F. J.; Rodríguez-Mirasol, J.; Rodríguez, J. J.; Cordero, T. *Transp. Porous Media* **2009**, *83*, 573-590.

(58) Barkauskas, J.; Stankevičienė, I.; Dakševič, J.; Padarauskas, A. *Carbon* **2011**, *49*, 5373-5381.

(59) Ye, F. M.; White, C. C.; Jin, Y. H.; Hu, X. G.; Hayden, S.; Zhang, X.; Gao, X. H.; Kavanagh, T. J.; Chiu, D. T. *Nanoscale* **2015**, *7*, 10085-10093.

(60) Lee, J.; Twomey, M.; Machado, C.; Gomez, G.; Doshi, M.; Gesquiere, A. J.; Moon, J. H. *Macromol*. *Biosci*. **2013**, *13*, 913-920.

(61) Miyazaki, T.; Ikegami, T.; Nagai, Y.; Nguyen, A.; Matsuzaki, Y.; Kobayashi, K.; Ceryak, S. *J. Cancer Ther.* **2013**, *4*, 944-952.

(62) Wijesinghe, D.; Arachchige, M. C.; Lu, A.; Reshetnyak, Y. K.; Andreev, O. A. *Sci*. *Rep*. **2013**, *3*, 1-7.

For Table of Contents Only